



Search for $H \rightarrow WW$ Production in the $e\tau$ and $\mu\tau$ Final States Using 5.9 fb^{-1}

The CDF Collaboration
URL <http://www-cdf.fnal.gov>
(Dated: July 15, 2010)

We present an update of the CDF search for a Standard Model Higgs boson decaying into WW^* in the final state with two charged leptons ($e\tau$, $\mu\tau$) and two neutrinos. Data are provided by the Tevatron $p\bar{p}$ collider at $\sqrt{s} = 1.96 \text{ TeV}$ and correspond to 5.9 fb^{-1} . In order to maximize the sensitivity, a Boosted Decision Tree is trained to separate the signal from the background using both event kinematics and τ identification observables. We expect 435 ± 70 background events in the $e\tau$ channel and 291 ± 43 events in the $\mu\tau$ channel and 1.07 ± 0.10 and 0.65 ± 0.06 signal events, respectively, for a Higgs mass of $165 \text{ GeV}/c^2$. In data we observe 446 $e\tau$ events and 295 $\mu\tau$ events. We set a 95% C.L. upper limit on $\sigma/\sigma_{\text{SM}}$ of 23.5 for a Higgs mass hypothesis of $165 \text{ GeV}/c^2$. The expected 95% C.L. upper limit for the same mass is 14.5. Results for fourteen other Higgs mass hypotheses ranging from $130 \text{ GeV}/c^2$ to $200 \text{ GeV}/c^2$ are also presented.

I. INTRODUCTION

The Higgs boson is introduced in the Standard Model to explain the electroweak symmetry breaking and the origin of boson and fermion masses. Current precision electroweak measurements constrain the mass of a standard model Higgs boson to be less than $157 \text{ GeV}/c^2$ (one-sided 95% C.L. upper limit) or $186 \text{ GeV}/c^2$ when including the LEP-2 direct search lower bound limit of $114.4 \text{ GeV}/c^2$ at 95% C.L [1].

The analysis presented in this note represents an update of the CDF search for $H \rightarrow WW^* \rightarrow \ell\ell'\nu\bar{\nu}$ where $\ell = e, \mu$ and $\ell' = \tau$. We use approximately 5.9 fb^{-1} of data produced by the Tevatron collider at $\sqrt{s} = 1.96 \text{ TeV}$ and collected by the CDF detector.

The analysis is based on events with one fully identified lepton of first or second generation and one fully identified hadronically decaying τ . Minimal event selection is applied to reduce the background while maintaining a large fraction of the signal. In order to increase the sensitivity a Boosted Decision Tree (BDT) [2] is used to further discriminate the signal from the background. The BDT uses both event kinematics and τ identification observables and it is trained for each mass hypothesis. A Bayesian method is used to calculate the 95% C.L. upper limit on the Higgs production cross section based on the predicted and observed BDT templates.

II. DETECTOR DESCRIPTION

The components of the CDF II detector relevant to this analysis are described briefly here; a more complete description can be found elsewhere [3]. The detector geometry is described by the azimuthal angle φ and the pseudo-rapidity $\eta = -\ln(\tan\vartheta/2)$, where ϑ is the polar angle of a particle with respect to the proton beam axis (positive z -axis). The pseudo-rapidity of a particle originating from the center of the detector is referred to as η_{det} . The trajectories of charged particles are reconstructed using silicon micro-strip detectors [4, 5] and a 96-layer open cell drift chamber (COT) [6] embedded in a 1.4 T solenoidal magnetic field. For $|\eta_{\text{det}}| \leq 1$, a particle traverses all 96 layers of the COT; this decreases to zero at $|\eta_{\text{det}}| \approx 2$. The silicon system provides coverage with 6 (7) layers with radii between 2.4 cm and 28 cm for $|\eta_{\text{det}}| < 1$ ($1 < |\eta_{\text{det}}| < 2$). Outside of the solenoid are electromagnetic (EM) and hadronic (HAD) sampling calorimeters segmented in a projective tower geometry. The first hadronic interaction length (λ) of the calorimeter, corresponding to 19-21 radiation lengths (X_0), uses lead absorber for measuring the electromagnetic component of showers, while the section extending to 4.5-7 λ uses iron to contain the hadronic component. The calorimeters are divided in a central ($|\eta_{\text{det}}| < 1$) and forward ($1.1 < |\eta_{\text{det}}| < 3.64$) region. Shower maximum detectors (SMX) embedded in the electromagnetic calorimeters at approximately 6 X_0 help in the position measurement and background suppression for electrons. Outside of the central calorimeters are scintillators and drift chambers for identifying muons as minimum ionizing particles.

III. LEPTON IDENTIFICATION

The data are collected with inclusive high- p_T lepton (electron or muon) triggers. We use the same data sample and 1^{st} - 2^{nd} generation lepton selection as the search for a Higgs boson decaying to two W bosons in [7].

All electrons and muons are required to be isolated such that the sum of the E_T for the calorimeter towers in a cone of $\Delta R = \sqrt{(\Delta\eta)^2 + (\Delta\varphi)^2} < 0.4$ around the lepton is less than 10% of the electron E_T or muon p_T . The transverse energy E_T of a shower or calorimeter tower is $E \sin\vartheta$, where E is the associated energy. Similarly, p_T is the component of track momentum transverse to the beam line.

Electron candidates are required to have a ratio of HAD energy to EM energy consistent with originating from an electromagnetic shower. The candidate electron has to be associated to a well-measured track satisfying $p_T > 10 \text{ GeV}/c$ that is fiducial to the central shower maximum detector (SMX) and matched to a central EM energy cluster. The candidate is also required to have a matching cluster in the SMX, minimal energy sharing between towers, and a ratio for shower energy E to track momentum p of less than $2.5 + 0.0015 E_T$.

Muons are identified by a charged track releasing a small amount of energy in the calorimeter and matched to a reconstructed track segment (“stub”) in the muon chambers. For $|\eta_{\text{det}}| < 1.2$, strict requirements on the number of tracking chamber hits and the χ^2 of the track fit are placed on the muon tracks in order to suppress kaon decay-in-flight backgrounds. In order to suppress background from cosmic rays, the track point of closest approach to the beamline must be consistent with originating from the beam line.

The hadronic decays of taus typically contain charged pions, neutral pions, and a tau neutrino. Since the decay products are collimated, a “signal” cone around a good quality track with $p_T > 10 \text{ GeV}/c$ is defined as $\alpha_{\text{sig}} = \min(0.17, 5/E^{\text{clu}} [\text{GeV}]) \text{ rad}$, where E^{clu} is the calorimeter energy of the candidate tau. Charged pions are reconstructed as tracks in the signal cone while neutral pions as calorimeter showers. In particular, the search is

based on τ 's with either 1 (1-prong) or 3 (3-prong) tracks such that the sum of the charges is ± 1 . Since the neutrino escapes detection, only partial reconstruction of the tau momentum is possible. A so called “visible momentum” is defined as the sum of the track momenta and neutral pion momenta in the signal cone. To be identified, τ 's must exhibit $E_T^{\text{vis}} > 15$ (20) GeV for 1-prong (3-prong) candidates. To suppress the large jet contamination, the visible mass is requested to be smaller than 1.8 (2.2) GeV/c^2 for 1-prong (3-prong) candidates. Muons mis-reconstructed as taus are rejected by imposing the ratio of energy to momentum to be larger than 0.8. Electrons are separated from taus using the relation between the electromagnetic fraction and the total calorimeter energy associated to the candidate: $\frac{E_{\text{tot}}}{\sum |\vec{p}|} (0.95 - E_{\text{em}}/E_{\text{tot}}) > 0.1$. Finally the following are the criteria for isolation, based on the “isolation” cone $\min(0.17, 5/E^{\text{clu}} [\text{GeV}]) < \alpha_{\text{iso}} < 0.52$ rad:

- track isolation, defined as the scalar sum of the p_T 's of all tracks with $p_T > 1 \text{ GeV}/c^2$ in the isolation cone: $I_{\text{trk}} < 2 \text{ GeV}/c$;
- no tracks with $p_T > 1.5 \text{ GeV}/c$ in the isolation cone;
- π^0 isolation, defined as the sum of the E_T 's of all π^0 's with $E_T > 1 \text{ GeV}$ reconstructed in the isolation cone: $I_{\pi^0} < 1 \text{ GeV}$.

The details about τ identification are documented in [8].

To identify the presence of neutrinos, we use the missing transverse energy $\cancel{E}_T = |\sum_i E_{T,i} \hat{n}_{T,i}|$, where the $\hat{n}_{T,i}$ is the transverse component of the unit vector pointing from the interaction point to the i -th calorimeter tower. The \cancel{E}_T is corrected for muons which do not deposit all of their energy in the calorimeter.

Candidate events are required to pass one of the online trigger selections implemented in three successively more stringent levels. The final central electron requirement is an EM energy cluster with $E_T > 18 \text{ GeV}$ matched to a track with $p_T > 8 \text{ GeV}/c$. Muon triggers are based on information from muon chambers matched to a track with $p_T > 18 \text{ GeV}/c$.

IV. BACKGROUNDS

The geometric and kinematic acceptance for the WW , WZ , ZZ , $W\gamma$, $Z/\gamma^* \rightarrow \tau\tau$, $Z/\gamma^* \rightarrow \ell\ell$, $t\bar{t}$, and $W + \text{jet}$ processes are determined using a Monte Carlo calculation of the collision followed by a GEANT3-based simulation of the CDF II detector response [9]. For the WW , WZ , ZZ , and Drell-Yan (DY) the generator used is PYTHIA [10], whereas for $W\gamma$ the generator described in [11]. The $W + \text{jet}$ background is estimated using ALPGEN [12] Monte Carlo interfaced with PYTHIA for the showering. We use the CTEQ5L parton distribution functions (PDFs) to model the momentum distribution of the initial-state partons [13].

A correction of up to 3% per lepton (electron or muon) is applied to the simulation based on measurements of the lepton reconstruction and identification efficiencies in data using Z decays. The MC τ identification efficiency is corrected at 3% level to match the efficiency in data [8].

The $Z/\gamma^* \rightarrow \ell\ell$ background contaminates the data sample if the flavor of one of the leptons is mis-assigned. The MC fake rate is corrected based on the rates measured in data using Z decays. The $W + \text{jet}$ process represents a background to the signal if the jet is mis-identified as a τ . The energy dependent rate of $\text{jet} \rightarrow \tau$ is corrected in MC based on the rate measured in jet triggered data. An additional correction factor of 0.704 ± 0.074 is applied to the $W + \text{jet}$ prediction in case of 1-prong τ candidates with no π^0 associated to the reconstructed τ .

Trigger efficiencies are determined from $W \rightarrow e\nu$ data for electrons and from $Z \rightarrow \mu^+\mu^-$ data for muons.

The background from di-jet and photon-jet production is estimated from a data sample of events with two identified leptons with same electric charge. Proper subtraction of electroweak contributions is applied to avoid event overcounting.

V. EVENT SELECTION

The $\tau\ell\nu_\ell\nu_\tau$ candidates are selected from events with two opposite-sign leptons. The electron or muon in the event is required to satisfy the trigger and have $E_T > 20 \text{ GeV}$ ($p_T > 20 \text{ GeV}/c$) for electrons (muons). The z -positions of the leptons at the point of closest approach to the beam-line are required to be within 4 cm of each other.

A loose event selection is applied to suppress the various background processes. The invariant mass of the dilepton system is constrained to the range $M_{\tau\ell} > 20 \text{ GeV}/c^2$ to reduce the contamination from low mass resonances. Requiring \cancel{E}_T above 20 GeV helps suppressing the Drell-Yan $Z/\gamma^* \rightarrow \ell\ell$, di-jet, and photon-jet processes with \cancel{E}_T due to resolution effects. Drell-Yan $Z/\gamma^* \rightarrow \tau\tau$ events exhibit real \cancel{E}_T and can be rejected if the angle between the \cancel{E}_T

Background component	$e\tau$	$\mu\tau$
dijet, γ +jet	4 ± 22	5 ± 16
$Z \rightarrow \tau\tau$	0.3 ± 0.2	0.5 ± 0.3
$Z \rightarrow \ell\ell$	7.7 ± 1.6	41.1 ± 6.2
W +jets	395 ± 66	229 ± 39
$W\gamma$	2.1 ± 0.3	1.2 ± 0.2
Diboson (WW, WZ, ZZ)	15.2 ± 2.3	10.1 ± 1.5
$t\bar{t}$	10.7 ± 2.6	4.8 ± 0.9
Total bkg	435 ± 70	291 ± 43
$gg \rightarrow H$ [$m_h = 160$ GeV/ c^2]	0.677 ± 0.085	0.408 ± 0.052
WH [$m_h = 160$ GeV/ c^2]	0.160 ± 0.022	0.099 ± 0.014
ZH [$m_h = 160$ GeV/ c^2]	0.104 ± 0.014	0.063 ± 0.009
VBF [$m_h = 160$ GeV/ c^2]	0.059 ± 0.009	0.036 ± 0.006
Total Signal	1.000 ± 0.089	0.606 ± 0.055
Data	446	295

TABLE I: Yields in the $e\tau$ and $\mu\tau$ channels (signal region).

and the dilepton transverse momentum is $\Delta\varphi_{\text{dilep}, \cancel{E}_T} > 1.5$ radians. The remaining dominant backgrounds due to WW and W +jet events are partially removed by imposing $\Delta\varphi_{\tau\ell} < 1.5$ radians.

The expected and observed yields after the selection cuts have been applied are shown in Table I.

VI. CONTROL SAMPLES

The background modeling and normalization are tested in several control samples, each of them targeting one specific component. The control samples are selected as follows:

- W-jet region:
 - $M_{\tau\ell} > 20$ GeV/ c^2 , $\cancel{E}_T > 20$ GeV, $\Delta\varphi_{\tau\ell} > 2$ radians;
- QCD region:
 - $M_{\tau\ell} > 20$ GeV/ c^2 , $\cancel{E}_T < 20$ GeV;
- $Z/\gamma^* \rightarrow \tau\tau$ region:
 - $M_{\tau\ell} > 20$ GeV/ c^2 , $\cancel{E}_T < 20$ GeV/ c^2 , $\Delta\varphi_{\ell, \cancel{E}_T} < 0.5$.

The expected background and the observed data show very good agreement in all control regions defined in the analysis.

VII. BOOSTED DECISION TREE

Given the large background contamination, advanced statistical techniques ought to be exploited to maximize the sensitivity to the SM Higgs boson production. We used a multivariate technique based on the Boosted Decision Tree. A decision tree is a binary tree classifier based on a set of rectangular cuts applied sequentially to the variables provided as input to the tree. A boosting procedure is applied to enhance the separation performance and make the decision robust against statistical fluctuations in the training samples: new trees are derived from the same training sample by reweighting the events which have been mis-classified. In this way, each tree is extended to a forest of trees and the final decision is taken by a weighted majority vote of the trees in the forest. The BDT structure has been optimized to maximize the signal-background separation: the maximum number of trees is set at 400, the maximum allowed depth for each tree is 5 and each node is required to have at least 400 events. At each node the cut value is optimized by scanning over the variable range with a granularity of 20 steps. We use the Gini index as a separation criterion and apply the adaptive boosting algorithm with a boosting parameter of 0.2.

The dominant background to the search is the W production when the gauge boson decays into an electron or a muon and an additional jet in the event is mis-identified as a τ . The BDT therefore should aim at discriminating the Higgs signal from such a process with a satisfactory efficiency. The best performance is achieved when the BDT is

Uncertainty source	WW	WZ	ZZ	$t\bar{t}$	$Z \rightarrow \tau\tau$	$Z \rightarrow \ell\ell$	$W+\text{jet}$	$W\gamma$	$gg \rightarrow H$	WH	ZH	VBF
Cross section	6.0	6.0	6.0	10.0	5.0	5.0			14.3	5	5	10
Measured W cross-section							12					
PDF Model	1.6	2.3	3.2	2.3	2.7	4.6	2.2	3.1	2.5	2.0	1.9	1.8
Higher order diagrams	10	10	10	10	10	10		10		10	10	10
Trigger Efficiency	0.5	0.6	0.6	0.6	0.7	0.5	0.6	0.6	0.5	0.5	0.6	0.5
Lepton ID Efficiency	0.4	0.5	0.5	0.4	0.4	0.4	0.5	0.4	0.4	0.4	0.4	0.4
τ ID Efficiency	1.0	1.3	1.9	1.3	2.1			0.3	2.8	1.6	1.7	2.8
Jet into τ Fake rate	5.8	4.8	2.0	5.1		0.1	8.8			4.2	4.0	0.4
Lepton into τ Fake rate	0.2	0.1	0.6	0.2		2.3		2.1	0.15	0.06	0.15	0.11
W+jet scale							1.6					
MC Run dependence	2.6	2.6	2.6				2.6					
Luminosity	5.9	5.9	5.9	5.9	5.9	5.9	5.9	5.9	5.9	5.9	5.9	5.9
Total	14.7	14.4	14.0	16.4	13.1	13.7	16.5	12.2	15.9	13.6	13.6	15.7

TABLE II: Systematic uncertainties on the backgrounds and signals for the $e\tau$ (expressed in %).

Uncertainty source	WW	WZ	ZZ	$t\bar{t}$	$Z \rightarrow \tau\tau$	$Z \rightarrow \ell\ell$	$W+\text{jet}$	$W\gamma$	$gg \rightarrow H$	WH	ZH	VBF
Cross section	6.0	6.0	6.0	10.0	5.0	5.0			14.3	5	5	10
Measured W cross-section							12					
PDF Model	1.5	2.1	2.9	2.1	2.5	4.3	2.0	2.9	2.6	2.2	2.0	2.2
Higher order diagrams	10	10	10	10	10	10		10		10	10	10
Trigger Efficiency	1.3	0.7	0.7	1.1	0.9	1.3	1.0	1.0	1.3	1.3	1.2	1.3
Lepton ID Efficiency	1.1	1.4	1.4	1.1	1.2	1.1	1.4	1.3	1.0	1.0	1.0	1.0
τ ID Efficiency	1.0	1.2	1.4	1.6	1.9				2.9	1.6	1.7	2.8
Jet into τ Fake rate	5.8	5.0	4.4	4.4		0.2	8.8			4.5	4.2	0.4
Lepton into τ Fake rate	0.06	0.05	0.09	0.04		1.9		1.2	0.04	0.02	0.02	0.04
W+jet scale							1.4					
MC Run dependence	3.0	3.0	3.0				3.0					
Luminosity	5.9	5.9	5.9	5.9	5.9	5.9	5.9	5.9	5.9	5.9	5.9	5.9
Total	14.8	14.6	14.6	16.2	13.1	13.6	16.6	12.1	16.0	13.8	13.7	15.8

TABLE III: Systematic uncertainties on the backgrounds and signals for the $\mu\tau$ (expressed in %).

trained on the $gg \rightarrow H$ signal against the $W + \text{jet}$ background. In particular, the discriminating power is enhanced when event based observables are accompanied by observables specific to the τ identification; the latter help to distinguish real τ leptons from τ candidates originating from jets. The distributions of the variables used as BDT input are presented from Figure 1 to Figure 4 in both the $e\tau$ and $\mu\tau$ channels. Examples of signal to background separation and BDT scores for three mass hypotheses are shown in Figure 5 and Figure 6.

VIII. SYSTEMATICS

Systematic uncertainties associated with the Monte Carlo simulation affect the Higgs, WW , WZ , ZZ , $t\bar{t}$, Drell-Yan, $W + \text{jet}$, and $W\gamma$ acceptances taken from the simulated event samples.

Uncertainties originating from lepton selection and trigger efficiency measurements are propagated through the acceptance calculation, giving uncertainties typically around 0.5% for the $e\tau$ channel and 1% for the $\mu\tau$ channel. The uncertainty due to the τ reconstruction and identification ranges between 1 and 3%, depending on the fraction of real taus in the sample. The fake rate of leptons into τ 's in the $Z/\gamma^* \rightarrow ee/\mu\mu$ sample introduces an uncertainty of the order of 2%. The uncertainty on the jet into τ fake rate affects primarily the $W + \text{jet}$ sample (9%).

We also assign an acceptance uncertainty of 10% due to potential contributions from higher-order effects, which is calculated in a WW sample as the difference between the leading-order (PYTHIA-based [10]) and next-to-leading order (MC@NLO [14]) acceptances.

The acceptance variations due to PDF model uncertainties is assessed to be on the order of a few percents using the 20 pairs of parton distribution functions (PDF) sets described in [15].

For the WW , WZ , ZZ , and $W + \text{jet}$ Monte Carlo samples that are not currently generated over the entire data run range, we take an additional uncertainty which accounts for the difference in the acceptance due to the use of a partial run range.

An additional systematic uncertainty of 1% on the $W + \text{jet}$ background originates from the scaling applied to the single-prong no- π^0 $W + \text{jet}$ component.

The uncertainties on the $WW/WZ/ZZ$ and $t\bar{t}$ cross sections are assigned to be 6% [16] and 10% [17, 18], respectively. Drell-Yan processes have an uncertainty of 5%. We normalize the $W + \text{jets}$ cross section to the inclusive W production cross section measured by CDF [19]. We quote the total systematic error on the measured value as a systematic uncertainty which results in an uncertainty of 12% on the $W + \text{jets}$ estimate. Uncertainties on the theoretical cross sections vary for the different Higgs production mechanisms. Associated production cross sections are known to NNLO, so the theoretical uncertainty on these cross sections is small, less than 5% [20]. Vector Boson Fusion (VBF) production is known only to NLO, so the residual theoretical uncertainty is higher (on the order of 10% [20]). Gluon fusion is a QCD process, so although it is known to NNLO, the corresponding theoretical uncertainty is still significant (14.3%). Further details on the estimation of these uncertainties are provided in [7].

In addition, all signal and background estimates obtained from simulation have a 5.9% uncertainty originating from the luminosity measurement [21].

Tables II and III report the full set of systematics sources estimated for this analysis.

IX. RESULTS

Since no excess is observed above the expected Standard Model backgrounds, the BDT scores are used as templates to set Bayesian 95% C.L. upper limits on the production cross section of the Standard Model Higgs. The 95% C.L. expected limits are determined with a set of 10000 Monte Carlo background-only experiments based on expected yields varied within the assigned systematics. Correlations between the systematics for different backgrounds are included. For each experiment a test statistic is formed from the difference in the likelihood value for the background-only model versus that for the signal plus background model. The results for the $e\tau$ and $\mu\tau$ channels are presented in Tables IV and V and Figures 7 and 8. The discrepancy between the observed and expected limits at $170 \text{ GeV}/c^2$ in the $\mu\tau$ channel has been thoroughly investigated and traced down to a statistical fluctuation of the data in a single bin of the corresponding BDT template. The $e\tau$ - $\mu\tau$ combined limits are shown in Table VI and Figure 9.

X. CONCLUSIONS

We performed a search for a Standard Model Higgs boson decaying into a pair of W bosons using the $e\tau$ and $\mu\tau$ signatures. In 5.9 fb^{-1} of data we expect 435 ± 70 background events in the $e\tau$ channel and 291 ± 43 events in the $\mu\tau$ channel and 1.07 ± 0.10 and 0.65 ± 0.06 signal events, respectively, for a Higgs mass of $165 \text{ GeV}/c^2$. In data we observe 446 $e\tau$ events and 295 $\mu\tau$ events. We set a 95% C.L. upper limit on $\sigma/\sigma_{\text{SM}}$ of 23.5 for a Higgs mass hypothesis of $165 \text{ GeV}/c^2$. The expected 95% C.L. upper limit for the same mass is 14.5.

Acknowledgments

We thank the Fermilab staff and the technical staffs of the participating institutions for their vital contributions. This work was supported by the U.S. Department of Energy and National Science Foundation; the Italian Istituto Nazionale di Fisica Nucleare; the Ministry of Education, Culture, Sports, Science and Technology of Japan; the Natural Sciences and Engineering Research Council of Canada; the National Science Council of the Republic of China; the Swiss National Science Foundation; the A.P. Sloan Foundation; the Bundesministerium für Bildung und Forschung, Germany; the World Class University Program, the National Research Foundation of Korea; the Science and Technology Facilities Council and the Royal Society, UK; the Institut National de Physique Nucleaire et Physique des Particules/CNRS; the Russian Foundation for Basic Research; the Ministerio de Ciencia e Innovación, and Programa Consolider-Ingenio 2010, Spain; the Slovak R&D Agency; and the Academy of Finland.

-
- [1] The LEP Electroweak Working Group, <http://lepewwg.web.cern.ch/LEPEWWG/>. 2
 - [2] A. Hoecker *et al.*, Proc. Sci **ACAT2007**, 040 (2007); L. Breiman *et al.*, *Classification and Regression Trees*, Wadsworth and Brooks, Monterey, CA, 1984. 2
 - [3] R. Blair *et al.*, The CDF Collaboration, FERMILAB-PUB-96/390-E (1996). 2
 - [4] A. Sill *et al.*, Nucl. Instrum. Methods A **447**, 1 (2000). 2
 - [5] A. Affolder *et al.*, Nucl. Instrum. Methods A **453**, 84 (2000). 2
 - [6] T. Affolder *et al.*, Nucl. Instrum. Methods A **526**, 249 (2004). 2
 - [7] D. Benjamin *et al.*, CDF Public Note 10232 (2010). 2, 6
 - [8] A. Aaltonen *et al.*, The CDF Collaboration, Phys. Rev. Lett. **103**, 201801 (2009). 3
 - [9] R. Brun *et al.*, CERN-DD-78-2-REV, CERN-DD-78-2 3
 - [10] T. Sjostrand, S. Mrenna, P. Skands, Peter, JHEP, **05** 026 (2006) 3, 5
 - [11] U. Baur, E.L. Berger, Phys. Rev. **D47** 4889-4904 (1993) 3
 - [12] M.L. Mangano *et al.*, J. High Energy Phys. **0307** 001 (2003) 3
 - [13] H.L. Lai *et al.*, CTEQ Collaboration, Eur. Phys. J. **C12** 375-392 (2000) 3
 - [14] S. Frixione and B.R. Webber, JHEP 06 (2002), hep-ph/0204244. 5
 - [15] S. Kretzer, H.L. Lai, F.I. Olness, and W.K. Tung, Phys. Rev. **D69**, 114005 (2004). 5
 - [16] J.M. Campbell and R.K. Ellis, Phys. Rev. **D60**, 113006 (1999). 6
 - [17] N. Kidonakis and R. Vogt, Phys. Rev. **D68**, 114014 (2003). 6
 - [18] M. Cacciari, S. Frixione, M.L. Mangano, P. Nason, and G. Ridolfi, JHEP **04**, 068 (2004). 6
 - [19] A. Abulencia *et al.*, J. Phys. G: Nucl. Part. Phys. (2007) 2457-2544. 6
 - [20] Tev4LHC Working Group, <http://maltoni.home.cern.ch/maltoni/TeV4LHC/SM.html>. 6
 - [21] D. Acosta *et al.*, Nucl. Instrum. Meth. **A494**, 57 (2002). 6

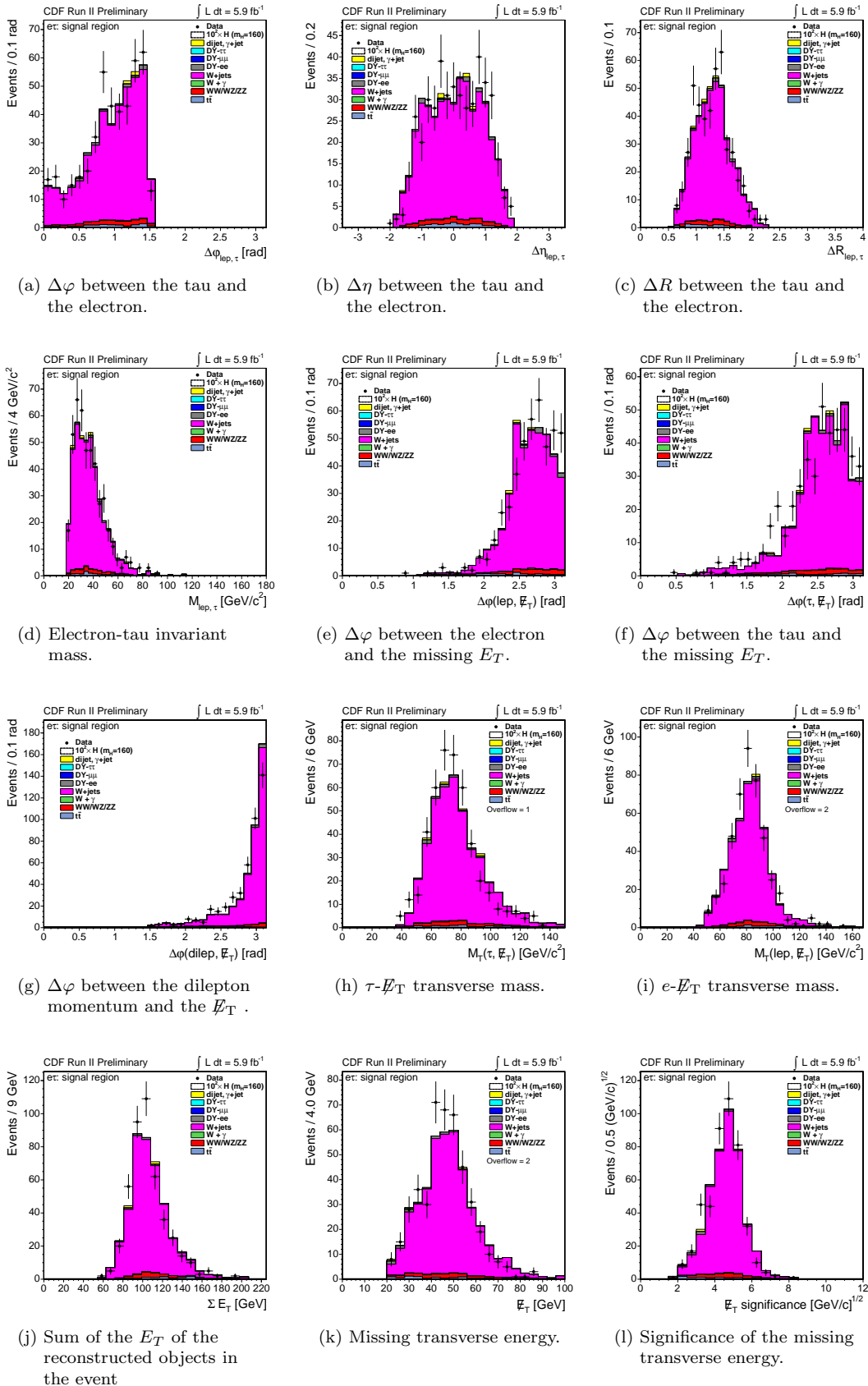


FIG. 1: $e\tau$ channel: data-MC comparison of the variables used in the BDT.

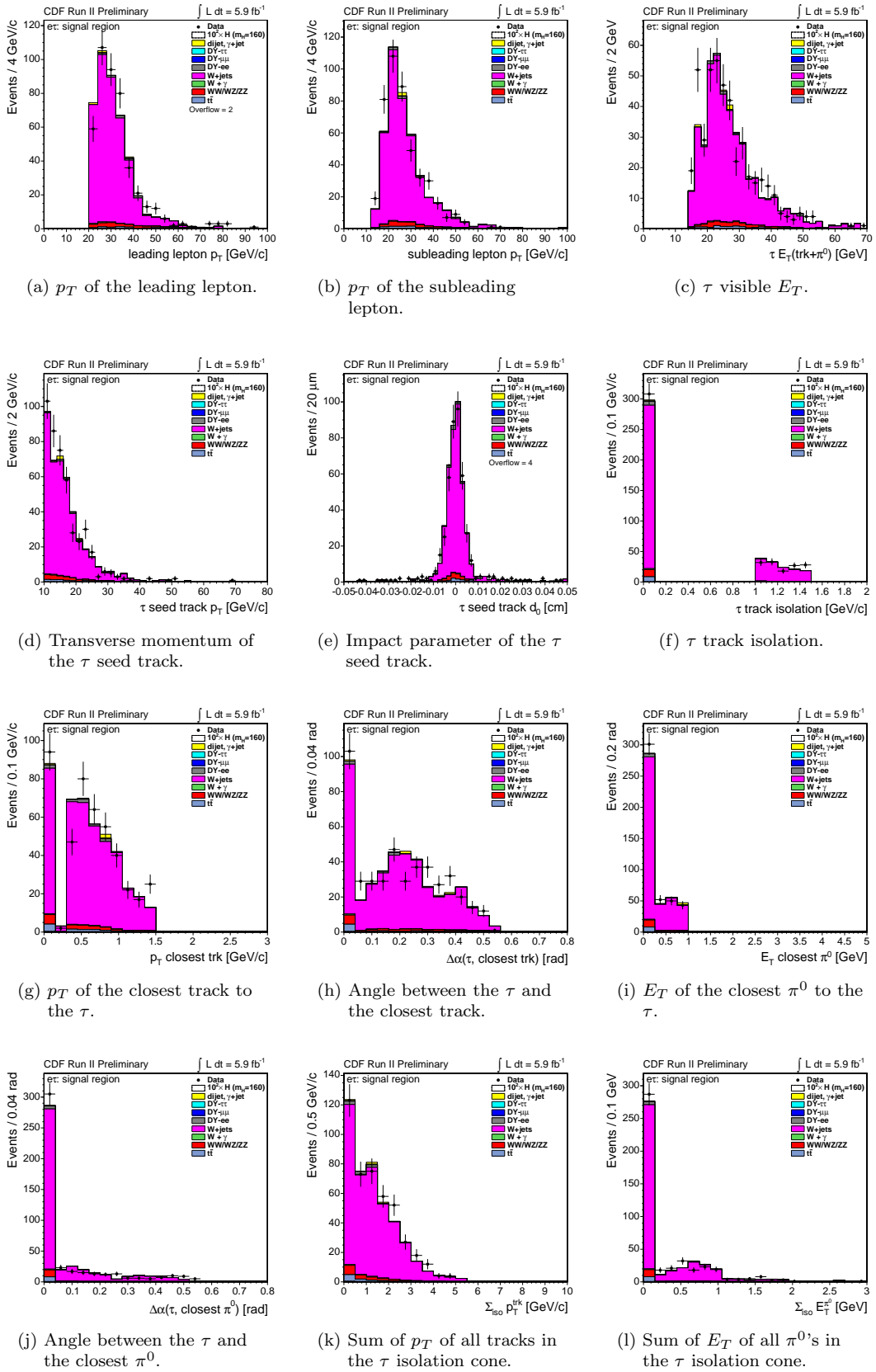
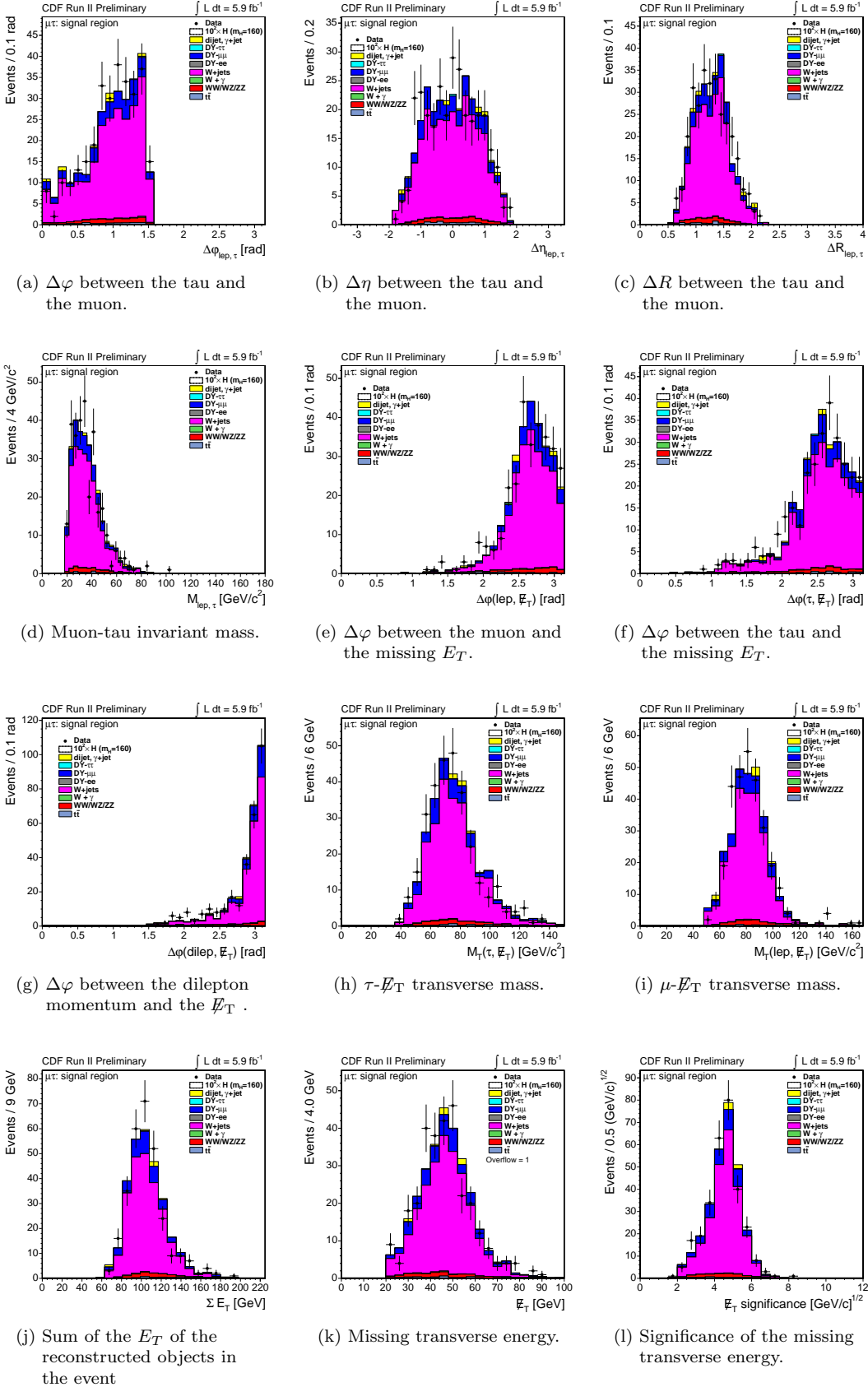
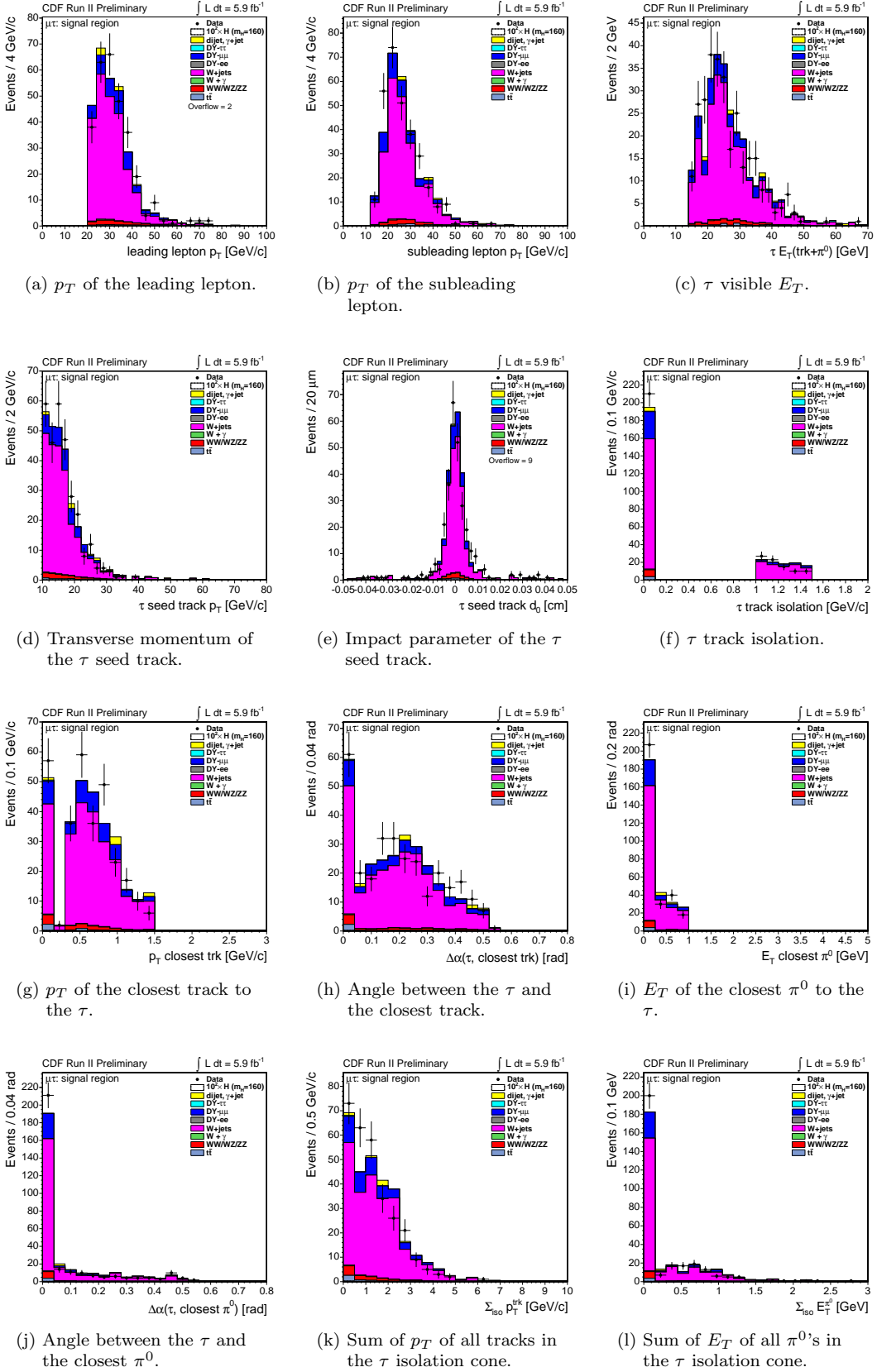
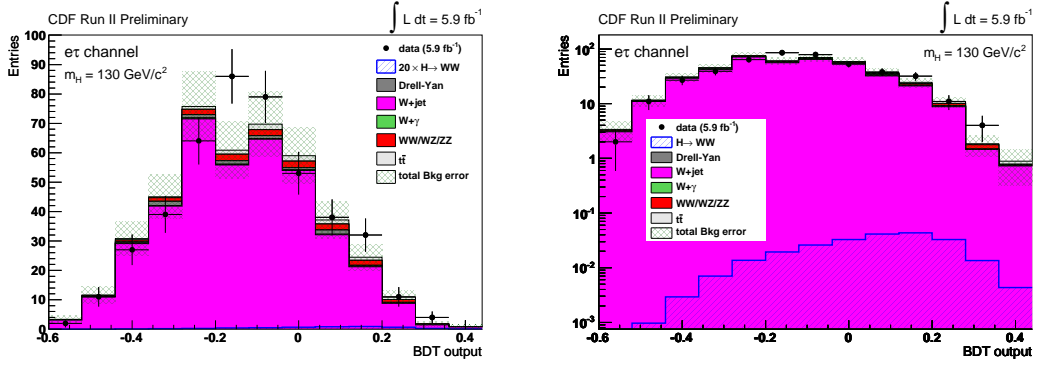
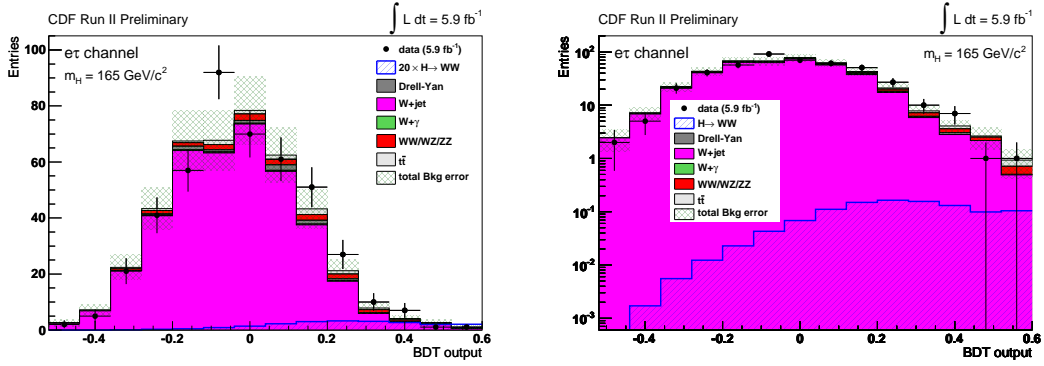
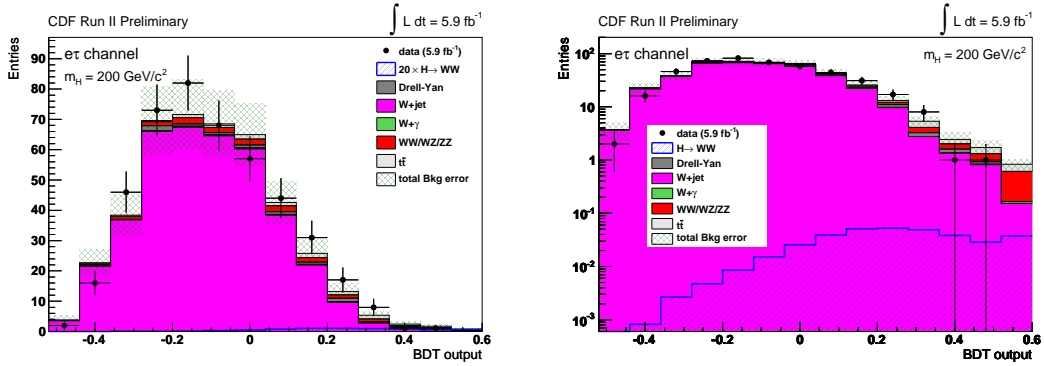
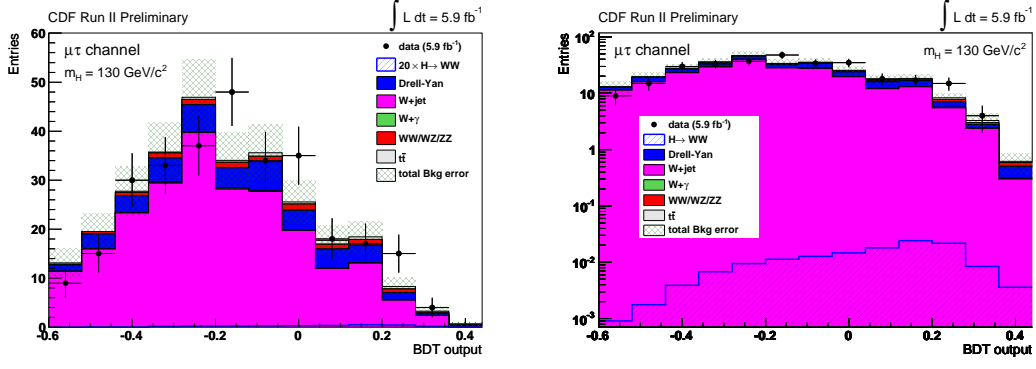
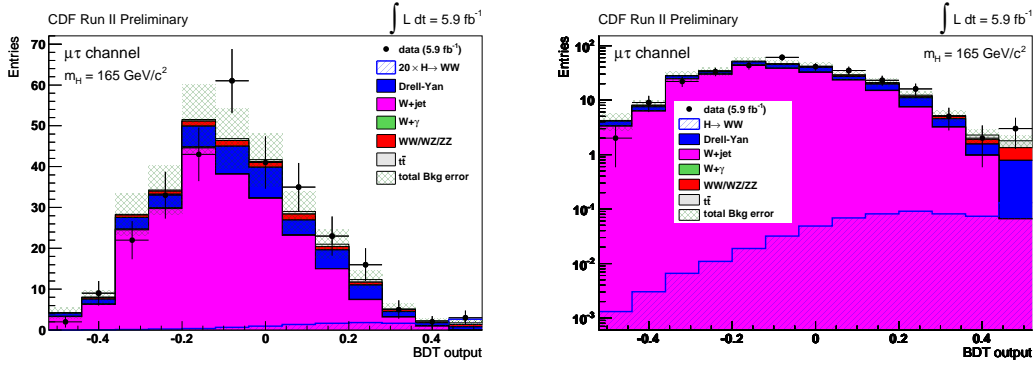
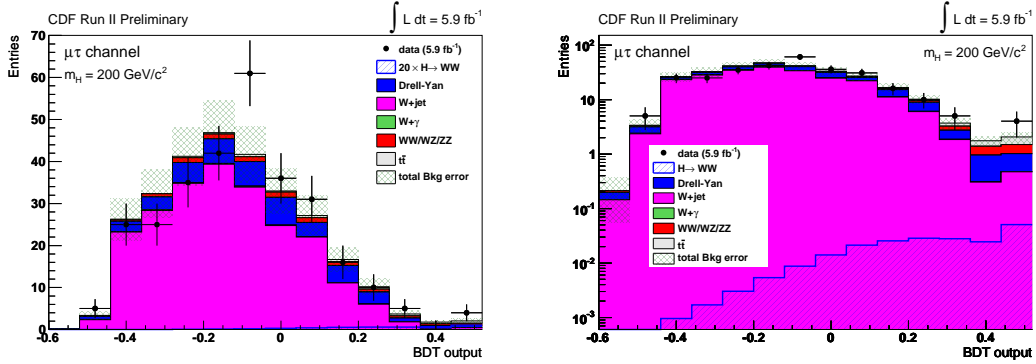


FIG. 2: $e\tau$ channel: data-MC comparison of the variables used in the BDT.

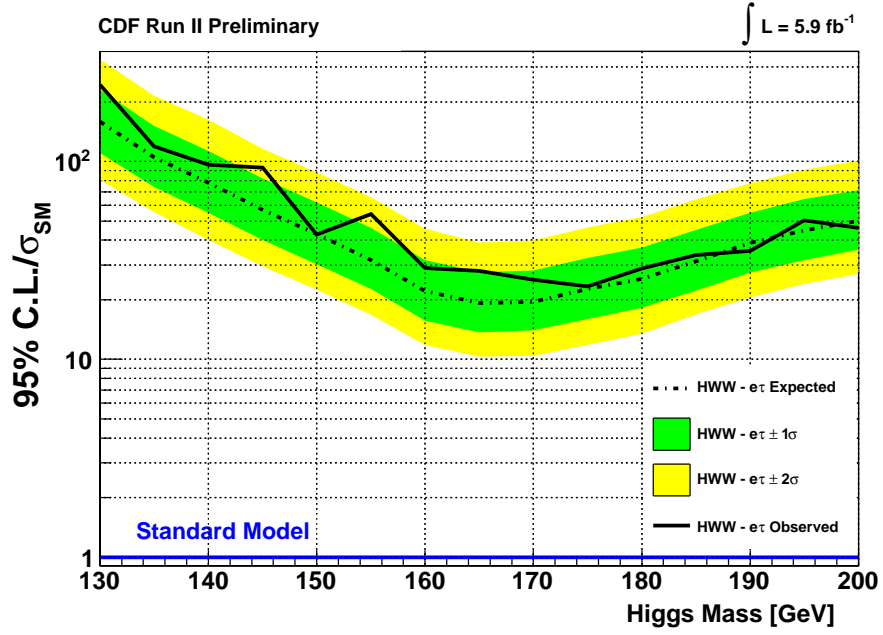
FIG. 3: $\mu\tau$ channel: data-MC comparison of the variables used in the BDT.

FIG. 4: $\mu\tau$ channel: data-MC comparison of the variables used in the BDT.

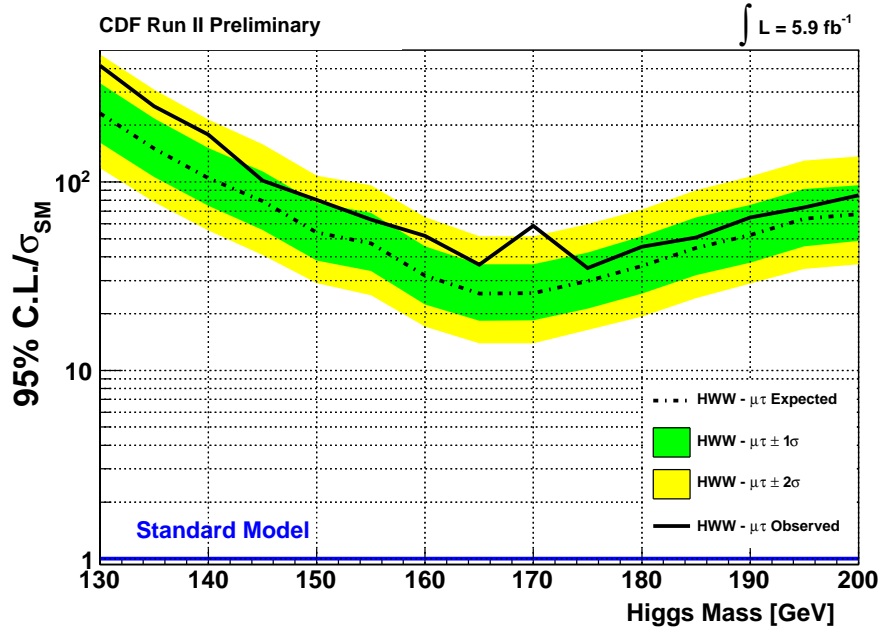
(a) $e\tau$ channel: $m_H = 130 \text{ GeV}/c^2$.(b) $e\tau$ channel: $m_H = 165 \text{ GeV}/c^2$.(c) $e\tau$ channel: $m_H = 200 \text{ GeV}/c^2$.FIG. 5: BDT templates for the Higgs mass hypothesis 130, 165, and 200 GeV/c^2 in the $e\tau$ channel.

(a) $\mu\tau$ channel: $m_H = 130 \text{ GeV}/c^2$.(b) $\mu\tau$ channel: $m_H = 165 \text{ GeV}/c^2$.(c) $\mu\tau$ channel: $m_H = 200 \text{ GeV}/c^2$.FIG. 6: BDT templates for the Higgs mass hypothesis 130, 165, and 200 GeV/c^2 in the $\mu\tau$ channel.

Higgs Mass [GeV/ c^2]	-2σ	-1σ	Median	$+1 \sigma$	$+2 \sigma$	Observed
130	80.7	110.3	158.8	230.2	327.2	243.9
135	55.6	74.5	105.2	151.6	215.1	119.2
140	40.0	55.1	78.2	112.8	162.9	96.2
145	29.5	40.0	57.0	81.9	115.7	93.0
150	22.5	30.2	43.0	62.2	88.1	42.8
155	16.8	22.7	31.8	46.1	65.9	54.3
160	11.8	15.7	22.1	31.8	45.8	28.9
165	10.3	13.7	19.2	27.6	38.9	28.0
170	10.4	14.0	19.5	28.1	39.8	25.3
175	11.8	16.0	22.7	32.5	46.4	23.3
180	13.5	18.2	25.5	36.7	52.3	28.8
185	16.9	22.2	31.2	45.0	64.1	33.7
190	20.6	27.4	38.7	55.1	77.8	35.3
195	24.1	31.8	44.8	64.6	90.9	50.4
200	27.0	35.9	50.2	71.4	100.9	46.1

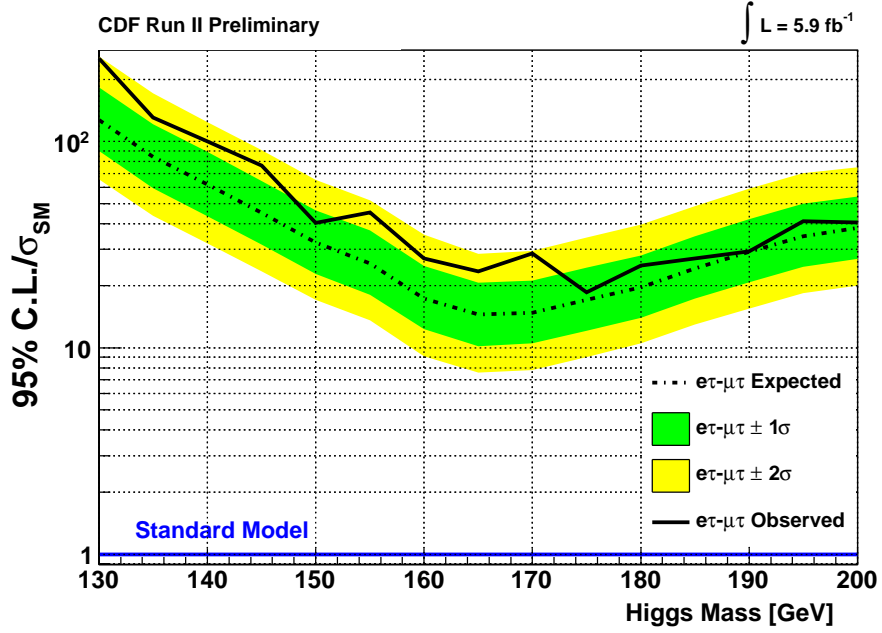
TABLE IV: Estimated and observed limits in the $e\tau$ channel.FIG. 7: Observed and expected limits for the $e\tau$ channel.

Higgs Mass [GeV/ c^2]	-2σ	-1σ	Median	$+1 \sigma$	$+2 \sigma$	Observed
130	118.4	161.2	230.9	334.2	474.4	412.9
135	78.3	106.2	150.3	217.2	309.0	251.9
140	55.3	74.6	104.8	150.8	213.9	177.7
145	40.8	55.6	78.9	113.5	158.5	101.4
150	29.0	38.3	53.8	77.4	108.1	80.2
155	25.0	33.6	47.2	68.4	95.8	63.2
160	17.1	22.4	31.8	45.5	65.0	51.8
165	13.9	18.3	25.6	36.6	51.3	36.3
170	13.9	18.4	25.7	36.6	51.4	58.3
175	16.4	21.3	29.7	42.1	59.5	34.9
180	19.3	25.6	35.7	51.4	71.2	45.3
185	24.2	31.9	44.5	64.7	90.4	50.6
190	28.8	37.3	52.1	75.3	107.0	64.6
195	34.5	45.4	63.6	91.8	129.7	73.3
200	36.6	48.6	67.5	96.1	136.4	84.7

TABLE V: Estimated and observed limits in the $\mu\tau$ channel.FIG. 8: Observed and expected limits for the $\mu\tau$ channel.

Higgs Mass [GeV/ c^2]	-2σ	-1σ	Median	$+1 \sigma$	$+2 \sigma$	Observed
130	65.4	89.8	127.1	182.3	257.6	252.3
135	43.6	59.4	84.2	121.3	171.5	130.5
140	32.0	43.5	61.9	88.9	124.2	100.2
145	23.5	31.7	45.1	64.4	90.7	76.4
150	17.1	22.8	32.3	46.3	65.1	40.4
155	13.6	18.1	25.7	37.0	51.9	45.2
160	9.1	12.3	17.3	24.9	35.4	27.1
165	7.6	10.2	14.5	20.7	28.6	23.5
170	7.8	10.5	14.8	21.2	29.5	28.7
175	9.0	12.1	17.1	24.5	34.2	18.6
180	10.5	14.0	19.7	28.0	39.6	25.0
185	13.0	17.3	24.3	34.8	48.5	27.1
190	15.5	20.8	29.2	42.1	59.2	29.4
195	18.4	24.7	34.8	50.0	70.2	41.0
200	20.0	27.0	38.2	54.1	75.0	40.5

TABLE VI: Combined observed and expected limits.

FIG. 9: Combined observed and expected limits for the $e\tau$ and $\mu\tau$ channels.